Research Square

Preprints are preliminary reports that have not undergone peer review.
They should not be considered conclusive, used to inform clinical practice,
or referenced by the media as validated information.

# Fabrication of 3D-Printed Hygromorphs Based on Different Cellulosic Fillers

**Matthias Langhansl**
Technische Universitat Munchen - Campus Straubing fur Biotechnologie und Nachhaltigkeit
**Jörg Dörrstein**
Technische Universitat Munchen - Campus Straubing fur Biotechnologie und Nachhaltigkeit
**Peter Hornberger**
Fraunhofer-Institut fur Integrierte Schaltungen
**Cordt Zollfrank** ( cordt.zollfrank@tum.de )
Technische Universitat Munchen - Campus Straubing fur Biotechnologie und Nachhaltigkeit
https://orcid.org/0000-0002-2717-4161

**Research**

**Keywords:** 3D Printing, actuation, bilayer, anisotropic swelling, cellulose, microcrystalline cellulose

**Posted Date:** September 15th, 2020

**DOI:** https://doi.org/10.21203/rs.3.rs-74821/v1

**License:** This work is licensed under a Creative Commons Attribution 4.0 International License.
Read Full License

**Version of Record:** A version of this preprint was published on January 29th, 2021. See the published version at https://doi.org/10.1186/s42252-020-00014-w.

# Abstract

The aim of this work is to characterize the moisture-dependent actuation behavior of bioinspired and additively manufactured hygromorphs based by following deductive and inductive design approaches. Fused Filament Fabrication is employed to print bilayered structures consisting of swellable active layers and rigid passive layers. The active layer is composed of a polylactic acid matrix filled with different hygroscopic cellulosic materials up to a filler content of 50 m%. Acrylnitril-Butadien-Styrol-Copolymer is used for the passive layer. The Fused Filament Fabrication process allows the generation of desired differential swelling properties in the composites upon moisture absorption. The moisture dependent actuation strain of the printed bilayers was determined by video analyses. Some influencing geometrical factors that contribute to the actuation were deduced from x-ray diffraction and micro computed tomography. The investigation of the mean cellulose microfibril orientation on the surface of the active layer suggested a preferential orientation with respect to printing direction. Furthermore, a gradient of cellulosic material within a single printed layer was observed, which indicates fiber sedimentation. Comparison with a thermomechanical model shows that the computational prediction of the moisture dependent actuation is considerably accurate for most selected cellulosic materials and filler contents.


# 1. Introduction

In nature plants have developed numerous kinds of movements to catch prey, to disperse seeds or to protect themself [1]. Many of these motions occur without an external source of energy. They are only driven by environmental humidity gradients [2]. The materials and design approaches inspired by these phenomena are often of non-renewable origin [3]–[5] while several approaches describe the use of wood [6], [7] or cellulose-based materials such as cottonid [8]–[10]. Hygromorphous structural materials respond to the relative humidity (Φ) of the environment by changing their dimensions, and thus their shape by swelling through the uptake of water. Pine cones are among the best known and well-described natural hygromorphs. The opening and closing of the ovuliferous scales is a result of the bilayered structure [11]–[13]. The different dimensional changes are caused by the almost perpendicular arrangement of cellulose fibrils in the adaxial (inner) and abaxial (outer) tissue. The humidity driven actuation of the scales can be described similar to thermally actuated bimetallic strips, where the two bound layers mechanically bend (mechanical energy) in response to differential expansion of the layers as a function of the temperature change (thermal energy). [14]. The classical modeling of the actuation of such bimetals according to Timoshenko 1925 [15] can be modified by replacing the actuation mechanism from temperature to humidity [14][16]. Herein the hygroexpansive strain is defined as the ratio between the changes in length to initial length as a function of moisture content [17]. By carefully characterizing geometry, mechanics, fluid transport, and evaporative flux of a porous medium the potential of natural and artificial hygromorphs can be estimated by employing hygromechanic models [14]. For the modeling of the actuation as a result of the sorption of moisture and dimensional changes a theoretical equation for thermo-bimetals was adjusted in the way that it is applicable for hygrosensitive actuators as reported earlier [14]. Following the assumption of Reyssat et al. the thickness of the active

layer $h_a$ and the passive layer $h_p$, their moduli $E_a$ and $E_p$, and their hygrometric coefficients of linear expansion in their unrestrained state $\alpha_a$ and $\alpha_p$ are independent of relative humidity Φ. Upon change in relative humidity ΔΦ the isotropic expansion is given by αΔΦ. The curvature change of the bilayer Δκ to calculate the theoretical displacement of moisture activated bilayers according to [14] is given by:

$$\Delta\kappa = \frac{\alpha\Delta\varphi f(m,n)}{h} \quad (1)$$

where

$$f(m,n) = \frac{6(1+m)^2}{3(1+m)^2 + (1+mn)(m^2 + \frac{1}{mn})} \quad (2)$$

and

$m = h_p/h_a$, $n = E_p/E_a$

Provided that $\alpha = \alpha_a - \alpha_p \neq 0$ and $RH_{t=0} \neq 100$ % the differential expansion of two interconnected layers leads to a bending at the tip of the bilayer.

Recently 3D printing of wood and wood constituents like cellulose and lignin has attracted much attention due to their benign properties regarding low-cost and natural origin [18]–[20]. Moreover, the fabrication of programmable materials by exploiting anisotropic swelling which is an inherent material property of underivatized cellulose allows the generation of 3D-printed hygromorphs. Such materials may find applications in smart textiles, autonomous robotics, biomedical devices, drug delivery and tissue engineering [21][22] and architecture [1]. However, further investigation is necessary to gain a better understanding of the behavior of the self-transforming composites. This consists in a detailed insight into the structure-transformation relationship which would allow the tailoring of hygromorphs preferably by adjusting the processing conditions. Additionally, the custom filament production allows for further experimentation on material composition as the use of different natural or modified cellulosic materials such as vulcanized cellulose and microcrystalline cellulose would impart different humidity-dependent dimensional changes [7]

# 2. Material And Methods

## 2.1 Materials

Polylactic acid (PLA, Ingeo 3251, NatureWorks LLC) and vinylacetate-vinylversatate-ethylene (Vac-VV-E, Vinnex LL 2505, Wacker Chemie AG) were used as received. The acrylonitrile-butadiene-styrene (ABS) filament (ABS black, Material 4 Print GmbH) has a mean diameter of 3 mm. As determined by microscopic image analysis microcrystalline cellulose (MCC, Alfa Aesar GmbH & Co. KG) exhibit an

average particle size of 27 µm, whereas Arbocel type F 140 K (AC, Rettenmaier & Söhne GmbH & Co. KG) have an average fiber length of 62 µm and were used as received.

### 2.2 Filament production

The filament production was carried out using a co-rotating twin-screw microcompounder (HAAKE MiniLab II, Thermo Scientific) equipped with a custom-made nozzle with a diameter of 1.5 mm. Filament extrusion was carried out at 190 °C at a screw speed of 50 rpm. The average residence time of the fiber-matrix mixture in the extruder was about 30 seconds. Commercial black ABS was used as a passive layer.

### 2.3 Fused Filament Fabrication (FFF)

Prior to the fabrication of the bilayers a digital model was created by using AutoCAD 2016 (Autodesk GmbH, Germany), figure 1 a. The model consisted of a passive layer of two perpendicularly oriented extrudate arrays of ABS, and of an active layer of PLA-cellulose compound. The bilayer model had the dimensions of 50 mm x 50 mm x 0.75 mm, with an overall thickness of the passive layer and the active layer of 0.5 mm and 0.25 mm, respectively. For the exact determination of the actuation the protrusion of the passive layer was removed. Models created in AutoCAD 2016 further processed with the AXON2 program (3D systems Inc.). A 3D-printer operating according to the FFF principle (3D Touch, 3D systems Inc.) was used to print the bilayers. The diameter of the nozzle opening was 0.25 mm. ABS and the active layer containing the PLA-cellulose composite were successively formed at 260 °C and 210 C, respectively. Each bilayer formulation was printed and characterized in duplicate

### 2.4 Theoretical model

According to equations (1) and (2), the determination of the elastic moduli of the individual layers Ea and Ep and the hygrometric coefficients of linear expansion αa and αp is needed. The elastic moduli of the individual layers were determined according to DIN EN 527 on six printed tensile bars (figure 1b) using a universal testing machine (smarTens, Karg Industrietechnik, Krailling, Germany). The results are given as the averages of six identically fabricated and tested specimens. The hygrometric coefficients of linear expansion were determined after water-immersion of printed specimens (100 mm x 2 mm x 0.5 mm) at room temperature for 1, 2, 3, 20 h and measuring the dimensional change using a digital caliper with an accuracy of 0.02 mm.

### 2.5 Determination of the actuation

The actuation (i.e. bending of the bilayer upon change in humidity) was followed by placing printed bilayers into a home-made climate chamber and subsequent video analysis. The humidity was established by placing dishes filled with water or different saturated salt solutions into the chamber. Humidity and temperature were measured constantly by a hygrometer 6100 (Electronic Temperature Instruments Ltd, Easting Close, UK). A tripod-mounted camera (Canon EOS 550D, Canon Germany GmbH, Krefeld, Germany) was connected to a PC. Images were taken at time intervals of 120 s with a total experimental time of 7 h (3.5 h for deflection and 3.5 h for provision). Each sample was determined in

duplicate, and the results are given as averages. The camera operated with following settings: shutter speed (Tv) 1/25, aperture (Av) 12, sensitivity of the image sensor ISO 400. Subsequently, the resulting 210 pictures were converted to an .avi video file with 30 frames per second. Finally, the videos were evaluated using the video analysis software Tracker (Douglas Brown, www.opensourcephysics.org), figure 2b.

### 2.6 Apparent cellulose orientation

#### 2.6.1 Cellulose orientation close to the surface

A Rigaku MniFlex 600 (Rigaku Corporation, Tokyo, Japan) X-ray diffractometer was used for the measurement. The sample was turned in steps of 10° after each measurement in order to determine a possible orientation of the fibres. An irradiation angle 2θ of 5° to 40° was investigated. The step size was 0.1° at a speed of 10° per min at a voltage of 40kV and a current of 15mA.

#### 2.6.2 Cross-sectional cellulose orientation

In order to investigate the orientation of individual fibers throughout the entire active layer, the samples were subsequently analyzed by micro computed tomography (µ-CT). The µ-CT measurement was carried out at the Fraunhofer Institute for Integrated Circuits IIS (Application Center CT in measurement technology (CTMT), Deggendorf). The scans were performed with a TomoScope HV 500 (Werth Messtechnik GmbH, Gießen Germany) tomograph. The parameters used for the measurements were: current 80 A, voltage 180 kV, 1600 steps for a 360° rotation and a total measurement time of 33 min. The resolution of the images was dependent on the measurement and ranged from 8 to 12.5 microns. Scans were conducted on AC bilayer specimens with fiber contents of 25% and 50% to investigate a possible re-orientation of the fibers by the printing process and a 10 cm long piece of filament with 50% Arbocel to examine the distribution of the fibers in the filament over the cross section prior to the printing process. Furthermore, a cylindrical shaped printed specimen was investigated, to compare the results with XRD measurements.

## 3. Results And Discussion

### 3.1 Bilayer Fabrication

Preliminary tests using pure and fiber filled PLA showed that the brittleness of the filaments prevented proper feeding. Thus the impact strength of the composites was modified by the addition of 10 m% of VAc-VV-E. Furthermore, the low glass transition temperature contributes to the processing at temperatures, preferably below the degradation of the cellulosic material starts. The microcompounder used for the fabrication of filaments was equipped with a custom-made nozzle with a diameter of 1.5 mm to compensate for the die swelling at the nozzle outlet, which is caused by entropic effects. A constant extrusion rate was maintained by setting the screw speed to 50 rpm and the uptake with a bobbin facilitated the compensation of pulsation. Filaments with a diameter of 3 mm ± 0.1 mm were produced, which was a prerequisite for reliable filament feeding throughout the printing process. A µ-CT-

scan of the extruded filament showed a homogeneous distribution of the cellulosic filler throughout its cross-sections, figure 3. Cavitiy formation could not be observed within the cellulose filled filament.

### 3.2 Actuation

Figure 4 shows an example of the time-dependent angular change of MCC bilayers with different amounts of fibers of 20 %, 40 %, and 50 % when exposed to a relative humidity of 75 %. All investigated actuation profiles showed a strong deflection directly after closing the climate chamber with 80%. The highest deflection rate of 5°/min observed in the first 60 minutes. Subsequently, the angular velocity gradually decreased until the end of the measurement after 210 min. The resetting upon removal of the salt solutions from the climate chamber was characterized by a higher absolute angular velocity of about 10°/min. A relationship between fiber content and total deflection was found with the highest angular deflections of 6.5° was observed at a fiber content of 50 % ($MCC_{50\%}$), followed by 5.1° ($MCC_{30\%}$), and 4.5° ($MCC_{20\%}$). A complete return to the initial dimension of the samples was not reached by any of the samples under investigation within 300 min. However, if the bilayer was stored at room temperature and a relative humidity of 30% a complete return was determined after approximately 10h. The MCC bilayers showed the highest angular deflection, both relative to the mass related fiber content and in absolute values as mentioned before with 6.5° observed at a fiber content of 50 % ($MCC_{50\%}$).

### 3.3 Theoretical Model

To understand the behavior of the actuators an analytical mechanical model was employed [10], which relates the curvature (κ) of the bilayer actuator to the humidity-induced strain of the material by equation (1). The results of the κ-calculations are shown in table 1. The model showed a good match between calculated and measured curvature changes. The differences were partly ascribed to errors in the course of determination of elastic moduli of the individual layers Ea and Ep and the hygrometric coefficients of linear expansion αa and αp and defects during the processing occurred. In the case of MCC30 % and MCC50 % good matches were observed between measured and calculated curvature changes. However, a poor match was observed for MCC20% which might be attributed to the comparatively lower fiber content which in turn leads to a reduced diffusion of water and therefore swellability of the microscale fibres.

***Table 1*** *Comparison of the measured curvature change Δκ measured of hygromorphs determined in a climate chamber and the modeled curvature change Δκcalculated by determination of elastic moduli (E) and hygrometric coefficients of linear expansion of the active layer ($\alpha_a$).*

| Sample | 25 % AC | 50 % AC | 20 % MCC | 30 % MCC | 50 % MCC |
|---|---|---|---|---|---|
| $\Delta\kappa_{measured}$ (°) | 3.1 | 2.6 | 4.5 | 5.1 | 6.5 |
| $\Delta\kappa_{modeled}$ (°) | 3.2 | 3.1 | 3.1 | 4.8 | 6.4 |
| E (MPa) | 458 | 407 | 289 | 247 | 478 |
| αa (-) | 0.011 | 0.012 | 0.006 | 0.010 | 0.01 |

### 3.4 Fiber orientation

The determination of the fiber orientation employs the evaluation of the full width at half maximum (FWHM) of the (002) cellulose crystalline plane [22]. Here FWHM is usually designated as Z and given in degrees whereas the preferential orientation of the crystalline regions is then given by Z/2. Thus, this method can give informations on the fiber orientation on the surface (limited by f.e. the excitation depth of the incident radiation) of the sample.

To investigate the orientation of the cellulose fibrils close to the surface the diffraction intensity of the 002 peak (a.u.) versus azimuthal angle (°) of the $AC_{50\%}$ specimen is shown in figure 5.

A Gaussian-shaped fitting curve yields the orientation angle Z/2 and gives information on fiber alignment. The results from x-ray diffraction analyses are summarized in Table 2.

Interestingly, the results obtained from XRD suggest that the orientation of cellulose fibrils close to the surface is perpendicular to the direction of printing. However, further investigation is needed which may also gain more understanding into the nonrecurring peak at 0° which we should assume for aligned discontinuous fiber-reinforced composites [22].

***Table 2*** *Fiber orientation (Z/2) along the preferred axis of the AC25 % and AC50 % hygromorphs. A comparison of the upperside and underside of fabricated AC25 % specimens showed slight differences for Z/2.*

| Sample | AC25 % Upperside | AC25 % Underside | AC50 % Upperside |
|---|---|---|---|
| Z (°) | 192 | 178 | 180 |
| Z/2 (°) | 96 | 89 | 90 |
| R2 | 0.77 | 0.96 | 0.93 |

To obtain additional information on the fiber orientation throughout the hygromorphs AC25% and $AC_{50\%}$

were studied by µ-CT, shown in figure 6. The AC25 % showed a graduated filler distribution with successively lower filler contents towards the bottom of the printed part. A possible explanation is that during printing the layer-by-layer deposition of successive filled material leads to a reheating of the layers and consequently to a gradual sedimentation of the filler to bottom. This graduation was not observed in the AC50 % specimen. Here, a homogeneous distribution of the cellulosic filler is clearly observed with relatively uniform distribution within a plane.

# 4. Summary

The aim of this work was to characterize the moisture-dependent actuation behavior of bioinspired and additively manufactured hygromorphs. Printable filaments were produced using a microcompounder which contained different quantities of pretreated and untreated cellulose fibers. The brittleness of the PLA was adjusted by the addition of a terpolymer of vinyl acetate-ethylene-vinyl versatate (10 m%), in order to improve the processability. FFF was used to successfully fabricate bilayered hygromorphous materials inspired by naturally occurring actuators. The analysis of these actuators suggest the presence of a specific preferential direction of the cellulose fibrils within the active layer, which might contribute to the actuation. Fiber sedimentation suggest to use mono-materials to create graded structures which in turn lead to actuation by omitting a rigid counterlayer. Finally, it could be shown that the actuation behavior of the printed hygromorphs can be estimated with high confidence by employing hygromechanic models.

# List Of Abbreviations

**FFF**: Fused Filament Fabrication

**ABS:** Acrylnitril-Butadien-Styrol-Copolymer

**PLA:** Polylactic acid

**XRD:** X-Ray diffraction

**µCT:** micro computed tomography

# Declarations

### Availability of data and materials

The datasets used and/or analysed during the current study are available from the corresponding author on reasonable request.

### Competing interests

The authors declare that they have no competing interests

### Funding

The authors thank the German Research Foundation (Deutsche Forschungsgemeinschaft, DFG) for funding the research project "Biomechanical qualification of the structure-optimized functional material Cottonid as an adaptive element" (WA 1672/23-1; ZO 113/22-1).

### Authors´ contributions

J. Dörrstein conceived the topic. P. Hornberger did the ct-scans. M. Langhansl drafted the article, conducted the Experiments and analized the data. C.Zollfrank supervised the project. The authors read and approved the final manuscript.

### Acknoledgements

Not applicable

# References

1. S. Poppinga *et al.*, “Toward a New Generation of Smart Biomimetic Actuators for Architecture,” vol. 1703653, no. Icd, pp. 1–10, 2017, doi: 10.1002/adma.201703653.
2. Y. Forterre, “Slow, fast and furious: Understanding the physics of plant movements,” *J. Exp. Bot.*, vol. 64, no. 15, pp. 4745–4760, 2013, doi: 10.1093/jxb/ert230.
3. L. Zhang, S. Chizhik, Y. Wen, and P. Naumov, “Directed Motility of Hygroresponsive Biomimetic Actuators,” *Adv. Funct. Mater.*, vol. 26, no. 7, pp. 1040–1053, 2016, doi: 10.1002/adfm.201503922.
4. B. Shin, J. Ha, M. Lee, K. Park, G. H. Park, T. H. Choi, K.-J. Cho, H.-Y. Kim, Hygrobot: A self-locomotive ratcheted actuator powered by environmental humidity. Sci. Robot. 3, eaar2629 (2018), Hygrobot: A self-locomotive ratcheted actuator powered by environmental humidity, doi: 10.1126/scirobotics.aar2629
5. S. Li and K. W. W. Wang, “Plant-inspired adaptive structures and materials for morphing and actuation: a review Related content Kinematic amplification strategies in plants and engineering Fluidic origami: a plant inspired adaptive structure with shape morphing and stiffness tuning,” *Bioinspir. Biomim*, vol. 12, p. 11001, 2017, doi: 10.1088/1748-3190/12/1/011001.
6. A. Holstov, B. Bridgens, and G. Farmer, “Hygromorphic materials for sustainable responsive architecture,” *Constr. Build. Mater.*, vol. 98, pp. 570–582, 2015, doi: 10.1016/j.conbuildmat.2015.08.136.
7. A. Papadopoulou, C. Guberan, N. Jhaveri, and D. Correa, “3D-Printed Wood : Programming Hygroscopic Material Transformations,” vol. 2, no. 3, pp. 106–116, 2015, doi: 10.1089/3dp.2015.0022.
8. R. Scholz, M. Langhansl, C. Zollfrank, and F. Walther, “Experimental study on the actuation and fatigue behavior of the biopolymeric material Cottonid,” *Mater. Today Proc.*, vol. 7, pp. 476–483, Jan. 2019, doi: 10.1016/J.MATPR.2018.11.112.

9. R. Scholz and J. Kristin, “Direction-dependent mechanical characterization of cellulose- based composite vulcanized fiber,” Materials Testing vol. 58, pp. 813–817, 2016, doi: 10.3139/120.110929.
10. Scholz R, Langhansl M, Zollfrank C and Walther F (2020) "Humidity-Sensing Material Cottonid – Microstructural Tuning for Improved Actuation and Fatigue Performance." Front. Mater. 7:156.doi: 10.3389/fmats.2020.00156
11. W. N. I. Harlow, W. Cote, and A. Day, “The opening mechanism of pine cone scales,” *J. For.*, pp. 538–540, 1964.
12. S. Poppinga *et al.*, “Hygroscopic motions of fossil conifer cones,” *Sci. Rep.*, vol. 7, no. December 2016, pp. 5–8, 2017, doi: 10.1038/srep40302.
13. S. Poppinga *et al.*, “Compliant Mechanisms in Plants and Architecture,” Springer, Cham, 2016, pp. 169–193.
14. E. Reyssat and L. Mahadevan,"Hygromorphs: from pine cones to biomimetic bilayers" J. R. Soc. Interface.6951–957, doi: 10.1098/rsif.2009.0184
15. S. Timoshenko, “Analysis of Bi-Metal Thermostats,” *J. Opt. Soc. Am.*, vol. 11, no. 3, p. 233, Sep. 1925, doi: 10.1364/JOSA.11.000233.
16. I. Burgert and P. Fratzl, “Actuation systems in plants as prototypes for bioinspired devices,” doi: 10.1098/rsta.2009.0003.
17. M. M. Hamedi *et al.*, “Electrically Activated Paper Actuators,” *Adv. Funct. Mater.*, vol. 26, no. 15, pp. 2446–2453, 2016, doi: 10.1002/adfm.201505123.
18. M. Kariz, M. Sernek, and M. K. Kuzman, “Use of wood powder and adhesive as a mixture for 3D printing,” *Eur. J. Wood Wood Prod.*, vol. 74, no. 1, pp. 123–126, Jan. 2016, doi: 10.1007/s00107-015-0987-9.
19. D. Wood, C. Vailati, A. Menges, and M. Rüggeberg, “Hygroscopically actuated wood elements for weather responsive and self-forming building parts – Facilitating upscaling and complex shape changes,” *Constr. Build. Mater.*, vol. 165, pp. 782–791, Mar. 2018, doi: 10.1016/j.conbuildmat.2017.12.134.
20. D. Correa *et al.*, “3D-Printed Wood: Programming Hygroscopic Material Transformations,” *3D Print. Addit. Manuf.*, vol. 2, no. 3, pp. 106–116, Sep. 2015, doi: 10.1089/3dp.2015.0022.
21. T. Gladman, “Precipitation hardening in metals,” *Mater. Sci. Technol.*, vol. 15, no. 1, pp. 30–36, 1999, doi: 10.1179/026708399773002782.
22. R. J. Kuriger, M. K. Alam, and D. P. Anderson, “Strength prediction of partially aligned discontinuous fiber-reinforced composites,” *J. Mater. Res.*, vol. 16, no. 1, pp. 226–232, 2001, doi: 10.1557/JMR.2001.0035.

# Figures

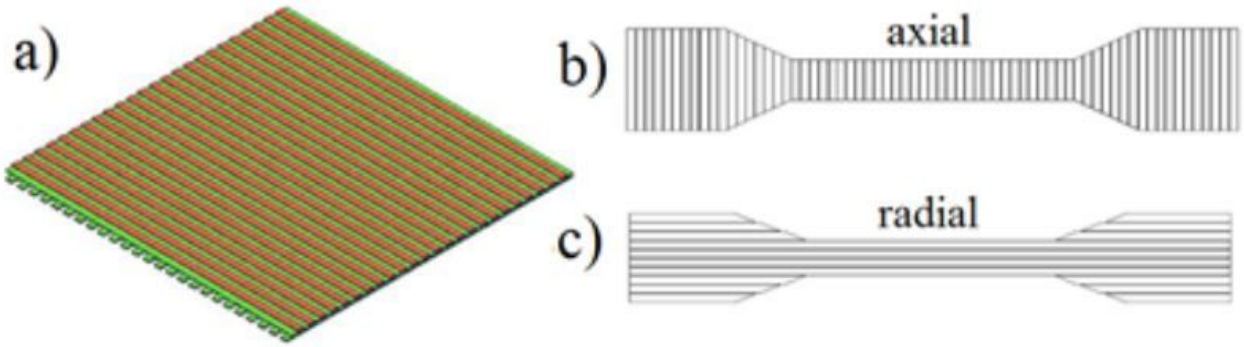


**Figure 1**

a) CAD-model of the PLA-based hygromorph consisting of mutually perpendicular passive layers (green) and an active layer (red). The length and width is 5 cm. b) and c) Schematic illustration of the axial and radial tensile bars with the corresponing print paths for the determination oft he elastic moduli

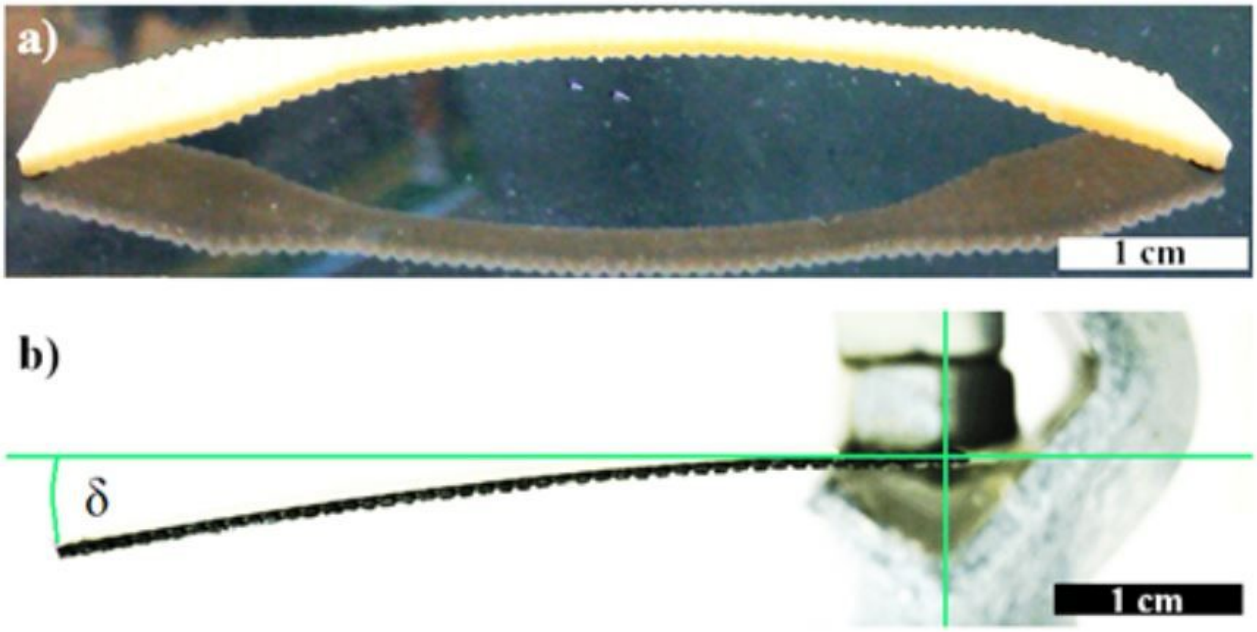


**Figure 2**

(a) Illustration of an axial AC25 % hygromorph after water-immersion for 2 min. (b) Example for the evaluation of the actuation of a 3D-printed after storage in a climate chamber at RH=75 %. The purple

horizontal line represents the position of the bilayer prior to the change in humidity at RH=30%

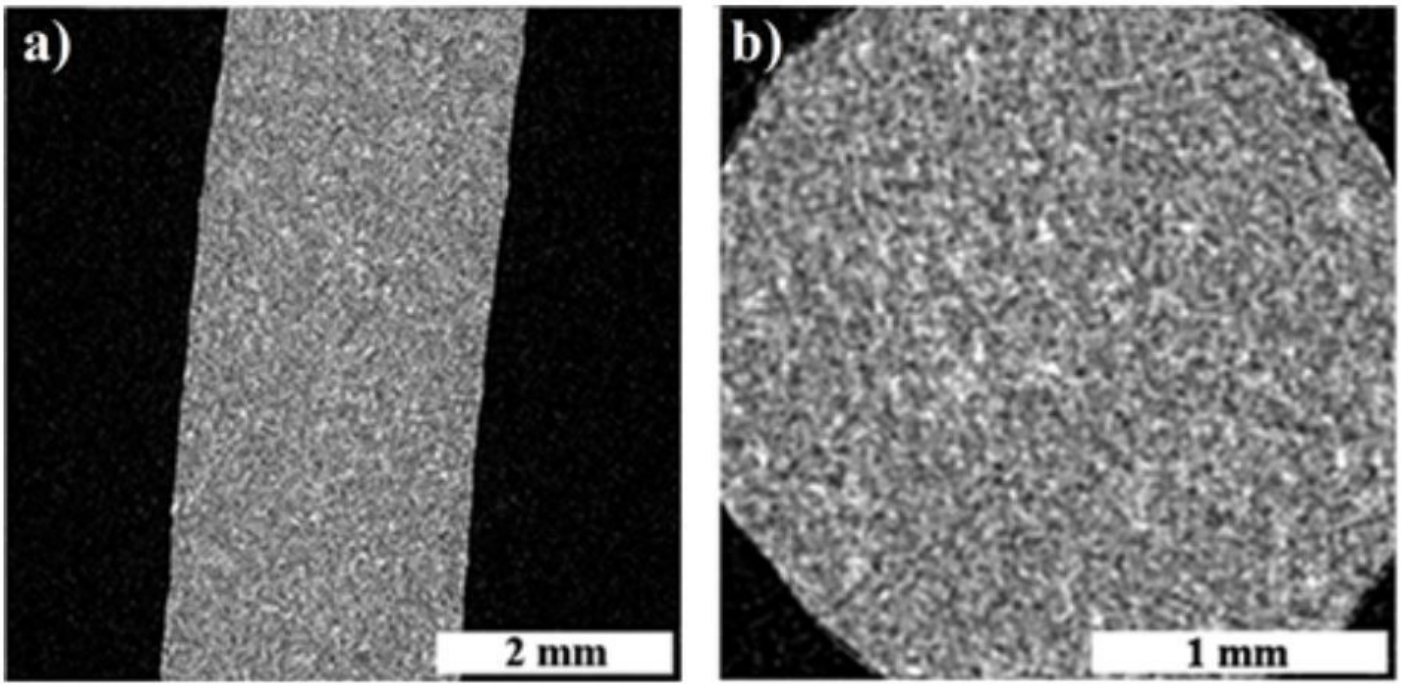


**Figure 3**

μ-CT scan of AC50 % filament prior to printing: General overview of the filament form sample a) and section through X-Y plane (b) Y-Z plane.

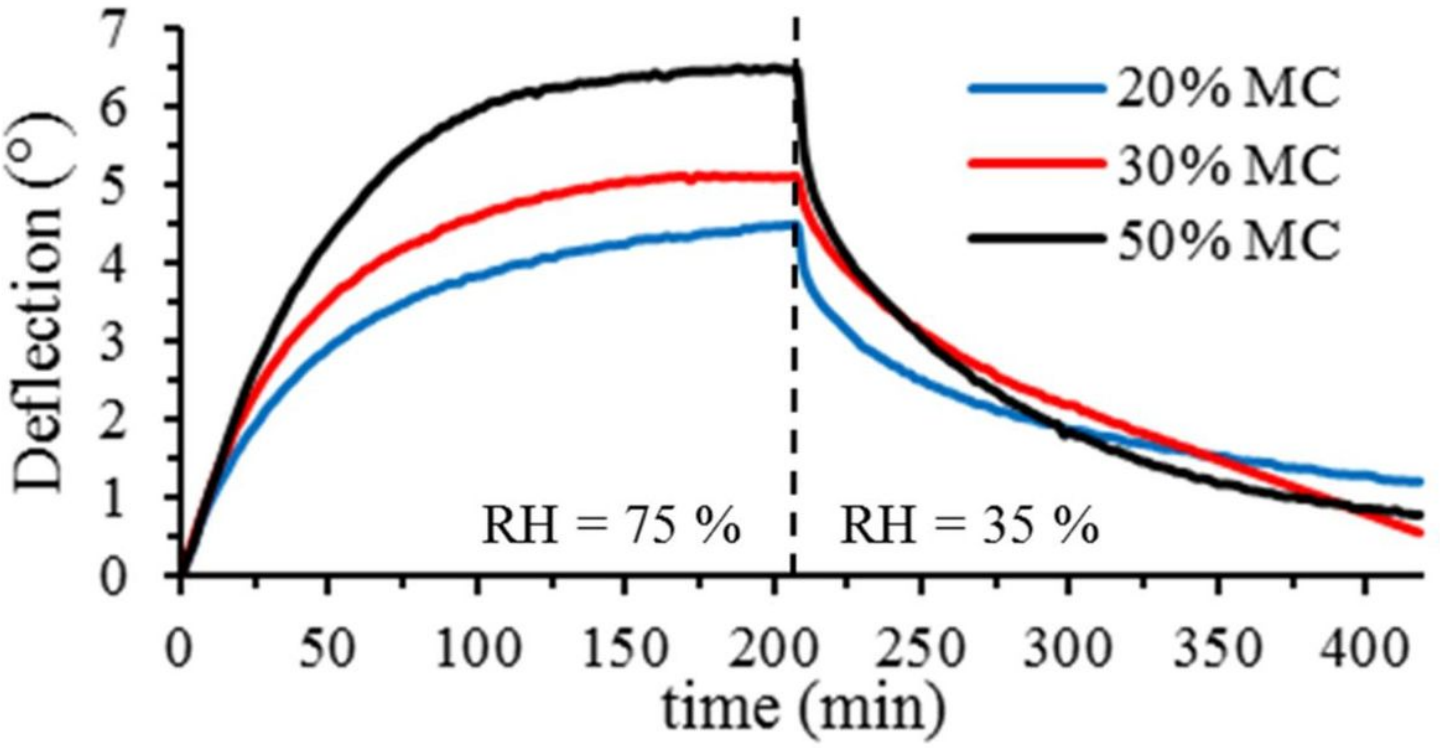

## Figure 4

Plot of the tip deflection versus time of printed MCC bilayers with MCC contents of 20 %, 30 %, and 50 % during exposure to a relative humidity of 75% for 210 min and subsequent drying in ambient air by removing the salt solutions from the climate chamber. The initial position of the equilibrated bilayer at ambient air was taken as the reference with Θ ambient air = 0.

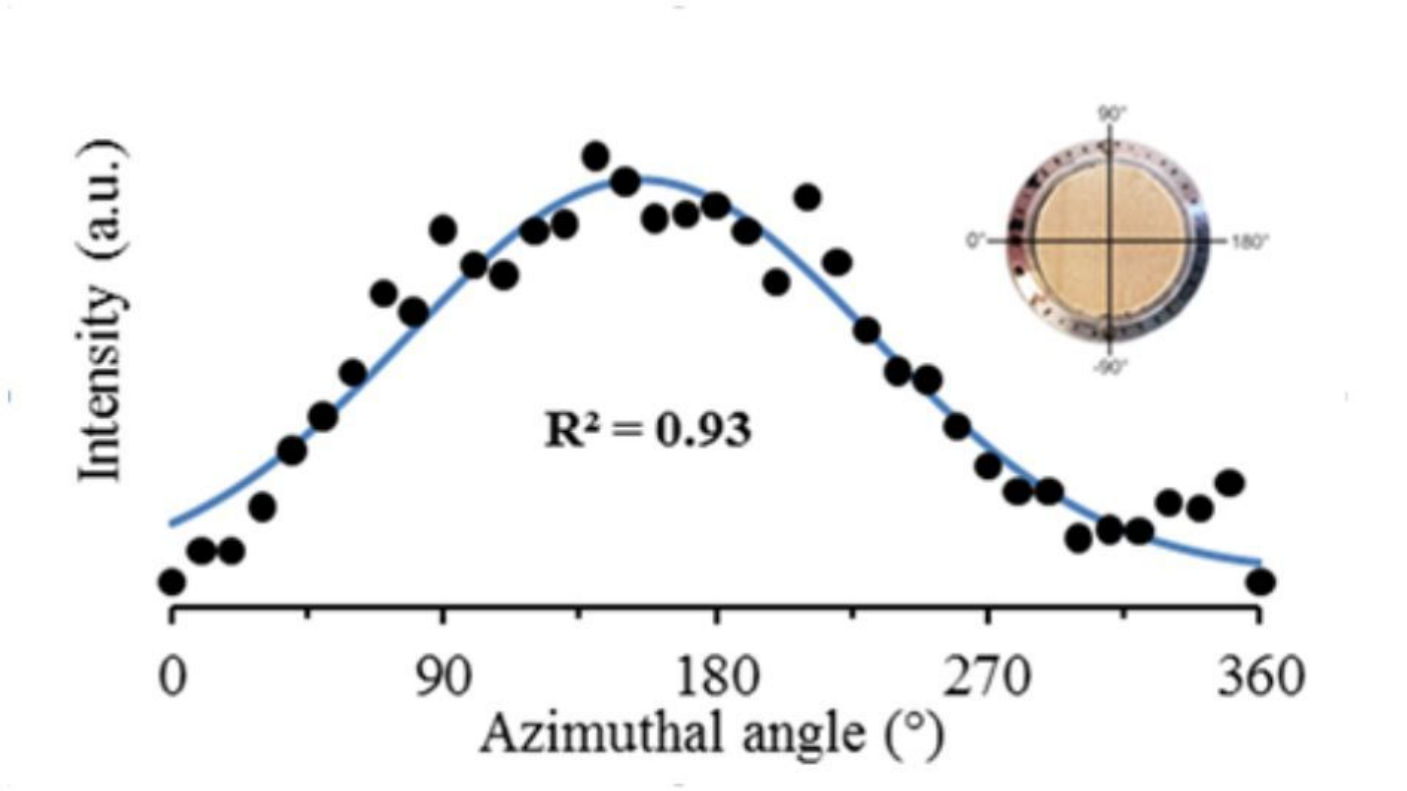


## Figure 5

Diffraction intensity (a.u.) versus azimuthal angle (°) of the AC50 % specimen and the Gauss-shaped fitting curve. The fiber alignment is calculated by the value of the angle (Z) for the width of the diffraction at one half the maximum intensity.

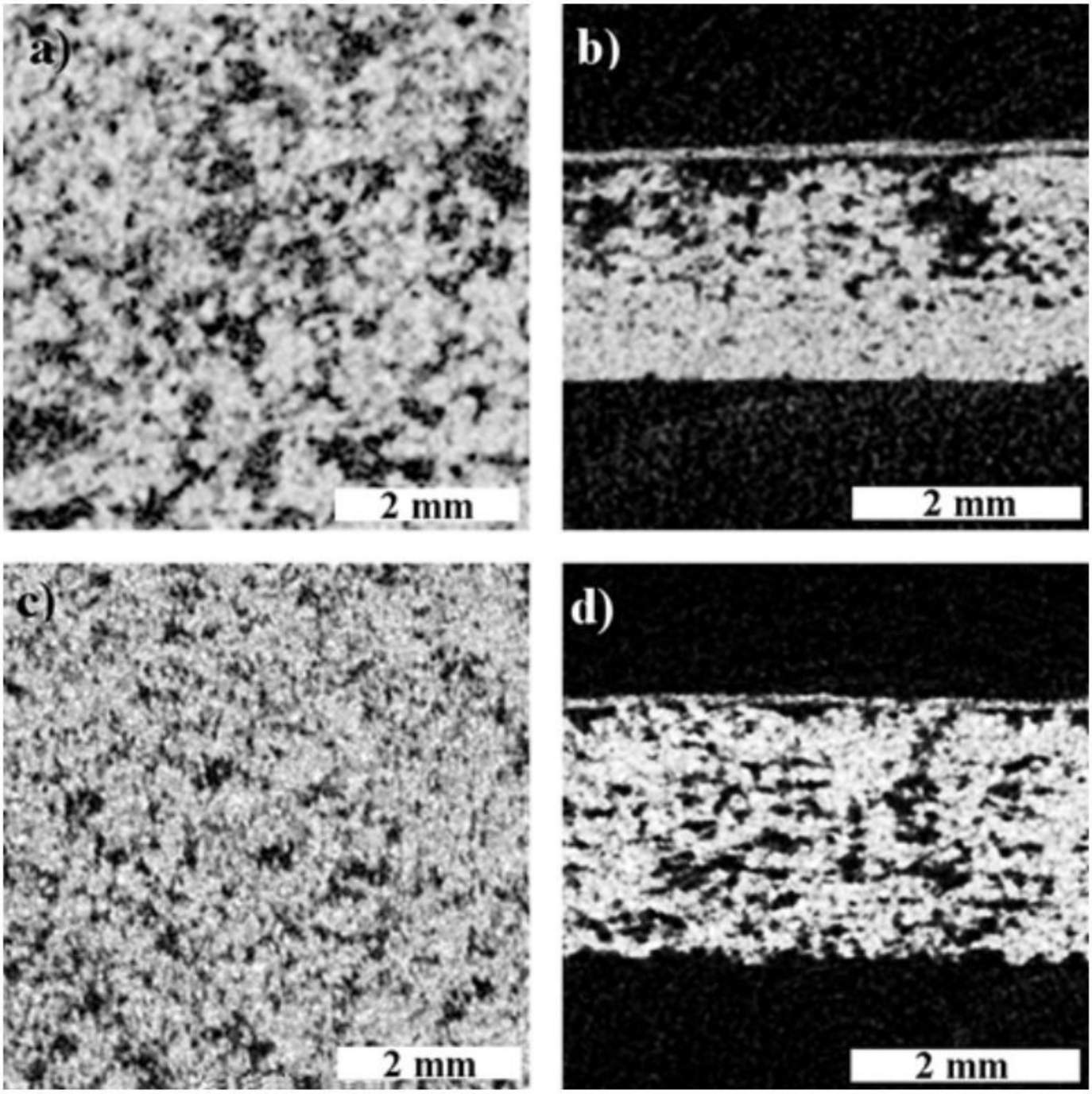


## Figure 6

Cross-sectional μ-CT images of 3D-printed XRD samples displaying the fibre dispersion within AC25% (a, b) and AC50% (c, d) as sections through the X-Y plane (a, c) and Y-Z plane (b, d)